Heliyon 7 (2021) e08218

Contents lists available at ScienceDirect

Heliyon

journal homepage: www.cell.com/heliyon

Research article

Nanocarbon hybrid for simultaneous removal of arsenic, iron and manganese ions from aqueous solutions

Mohamed A. Embaby [a], Shimaa M. Abdel Moniem [b], Nady A. Fathy [c], Ahmed A. El-kady [a,*]

[a] Food Toxicology and Contaminants Department, National Research Centre, 12622 Dokki, Giza, Egypt
[b] Water Pollution Research Department, National Research Centre, 12622 Dokki, Giza, Egypt
[c] Surface and Catalysis Laboratory, Physical Chemistry Department, National Research Centre, 12622 Dokki, Giza, Egypt

ARTICLE INFO

Keywords:
Nanocarbon hybrid
As
Fe
Mn
Adsorption
Isotherm

ABSTRACT

Heavy metal contamination is a severe problem with serious ecological and human health effects due to its toxic effect and tendency to accumulate throughout the food chain. Batch experiments were conducted to investigate the simultaneous removal of arsenic, iron and manganese ions from aqueous solutions using Nanocarbon hybrid (NCH). Nanocarbon hybrid (NCH) of carbon xerogel decorated with 1wt% multi-walled carbon nanotubes was prepared by carbonization at 850 °C for 2 h. The TEM, SEM, EDX, FTIR, and N_2 adsorption-desorption measurements were used to characterize the prepared NCH. NCH is enriched with surface oxygen functional groups and micropores as well as it have total surface area of 162 m^2/g and total pore volume of 0.129 cm^3/g. The adsorption of metal ions onto NCH, which confirmed by EDX, happened quickly, with 30%, 97%, and 41% of As, Fe, and Mn adsorbed in less than 10 min, however the equilibrium time was achieved in less than 30 min. The maximum adsorption capacities for As, Fe, and Mn ions onto NCH were 20, 48, and 21 mg/g, respectively. The experimental adsorption results of the three metal ions showed linearly fitting with Freundlich isotherms. In addition, the computed adsorption energies for Fe, Mn, and As ions were 4.08, 1.95, and 2.42 kJ/mol, indicating physical adsorption. NCH are easily regenerated and reusable sorbent owing to the adsorption–desorption studies. Conclusively, NCH is promising material for removing mixture of metal ions from aqueous media.

1. Introduction

Heavy metals, unlike organic contaminants, are not created; they are found naturally in the earth's crust. Heavy metals are released into the environment by a variety of industrial sectors, including textiles, pigments, plastics, mining, electroplating, and metallurgical processes, and are classified as persistent environmental contaminants since they can't be destroyed or degraded. Heavy metal contamination is a severe problem with serious ecological and human health effects due to its toxic effect and tendency to accumulate throughout the food chain (Montazer-Rahmati et al., 2011; El-Kady and Abdel-Wahhab, 2018). Manganese is toxic to the brain, and long-term exposure to excessive manganese levels has been linked to nervous system toxicity, resulting in a state similar to Parkinson's disease (Kwakye et al., 2015). Inorganic arsenic is classified within the group (1) as a carcinogen in humans (IARC, 2012). Bowen's disease (carcinoma in situ) and skin squamous cell carcinoma (SCC) are two malignancies that can result from long-term arsenic exposure (Verhave et al., 2019: Lu et al., 2020). Kumasaka et al. (2013) revealed for the first time that co-exposure to arsenic and iron increased carcinogenicity, with iron synergistically enhancing the arsenic carcinogenic effect. Maximum contamination level (MCL) for arsenic is set by EPA and WHO as 0.01 mg/L for drinking water. For Fe, 0.3 mg/L is established as a secondary drinking water regulation from EPA (EPA, 2018; WHO, 2008). A maximum acceptable concentration (MAC) of 0.1 mg/L is proposed for total manganese in drinking water by Federal-Provincial-Territorial Committee on Drinking Water (FPTCDW, 2016). European Union has recommended the levels of 0.2 mg/L and 0.05 mg/L for Fe and Mn, respectively (EU, 1998). Groundwater contamination by trace metals, particularly Fe, As, and Mn, has been existed globally, which occurred naturally or associated with anthropogenic activities (Lotfi et al., 2020; Malakootian et al., 2020). In the western Nile Delta region of Egypt, groundwater from 108 wells was examined for trace metals. Fe and Mn were found to be above the allowed limits (Sharaky et al., 2016). Furthermore, considerable and minor trace elements have been found in groundwater in Egypt's Northwest Sinai (El Alfy and Merkel, 2010; El Alfy, 2013). Dissolved iron and manganese

* Corresponding author.
E-mail address: aelkady16@gmail.com (A.A. El-kady).

https://doi.org/10.1016/j.heliyon.2021.e08218
Received 28 July 2021; Received in revised form 25 September 2021; Accepted 15 October 2021
2405-8440/© 2021 The Authors. Published by Elsevier Ltd. This is an open access article under the CC BY-NC-ND license (http://creativecommons.org/licenses/by-nc-nd/4.0/).

from sedimentary deposits are released to groundwater under reducing conditions at Bahariya Oasis in the Western desert. Several treatment technologies have been investigated to remove trace metals from different matrices of the environment, e.g. chemical precipitation, electrodialysis (Liu et al., 2013), ion exchange (Zhao et al., 2019), reverse osmosis (Carolin et al., 2017), coagulation and flocculation (Visa, 2016) have been established and characterized as costly and has a limited efficiency for metal remediation (Xu et al., 2017). Furthermore, the ability and capability of heavy metals bioremediation has been restricted and affected by several factors such as temperature, pH, metal toxicity, and others (Igiri et al., 2018; Sanad et al., 2021). On the other hand, adsorption techniques have been widely used for most organic and inorganic contaminants due to large surface area, high textural porosity, and functional groups, which boost the adsorption capacity for their targets (Embaby et al., 2017). Furthermore, since adsorption is typically reversible, adsorbents can be regenerated using appropriate desorption processes. In this regard, the adsorption heavy metals and other pollutants onto carbon-based nanomaterials such as carbon nanotubes (CNTs), graphene, graphene oxide and their composites exhibited superior removal than using traditional adsorbents such as activated carbons and clays (El-Kady et al., 2009; Ihsanullah et al., 2016; Lingamdinne et al., 2016; Wang et al. 2017, 2019; Xu et al., 2018). From these studies, CNTs and graphene materials are outstanding adsorbents to uptake different heavy metals from wastewater due to their excellent properties like unique hollow and layered structures which enable them to interact with organic molecules through several interactions which include non-covalent forces, e.g., $\pi-\pi$ stacking interactions, hydrogen bonding, van der Waals forces, hydrophobic interactions and electrostatic forces. Carbon xerogels (CXs) are composed of interconnected nodules of carbon spheres at nanometer scale with micro-mesoporous structure (Girgis et al., 2011). Use of CXs materials alone has appeared high adsorption capacities of dyes and Cu (II) ions with slow in diffusion and adsorption rates (Girgis et al. 2011, 2012). In order to enhance the diffusion and adsorption rates, Shouman and Fathy (2018) prepared microporous nanohybrid of CX decorated with MWCNTs as CX/MWCNTs that was prepared from chemical vapor deposition of camphor solid during carbonization of rice straw loaded with iron and nickel oxides as catalysts. From this point of view, we are looking to use nano carbon material to sequester heavy metals from aqueous solution. The adsorption of trace metals in single metal solutions has been extensively studied (Girgis et al., 2009; Ibrahim et al., 2013; El-Kady et al., 2016); however, few publications have been devoted to the studies of simultaneous adsorption of metal ions from aqueous solutions (Bohli et al., 2017; Fang et al., 2018; He et al., 2018; Prelot et al., 2018; Liu et al., 2020). Therefore, the aim of current study is to investigate the ability of nanocarbon hybrid (NCH) to eliminate As, Fe, and Mn from aqueous solution under various conditions (contact time, pH, dose, initial metal concentration). The efficiency of the produced NCH in terms of regeneration and reusability was tested against a mixture of As, Fe, and Mn.

2. Materials and methods

2.1. Chemicals and reagents

Ferric chloride ($FeCl_3$, with 99.8% purity, Fisher Chemical), Arsenic (III) oxide, (As_2O_3), Manganese sulfate monohydrate ($MnSO_4$ H_2O) $\geq$99.0%, Sigma-Aldrich), Hydrochloric acid (37 %) and sodium hydroxide pellets (98 %) were supplied by Fluka (Germany). Resorcinol (Panreac, 99%), formaldehyde (Adwic, 36–38%), methanol (Sigma-Aldrich, 99%), sodium carbonate and bicarbonate (POCH SA, 99%) and sodium dodecyl sulfate (SDS, Sigma-Aldrich, 98%) as an anionic surfactant were purchased and used without prior purification. A Laboratory-made multiwalled carbon nanotube sample (CNT) with outer diameters ranging from 22 to 66 nm and a specific surface area of 35 m^2/g has been used in the current study. The CNT sample was prepared by chemical vapor deposition of camphor as a carbon source onto hydrothermally treated rice straw catalyst support loaded with iron and nickel oxides for 30 min at 850 °C, as reported elsewhere (Fathy, 2017).

2.2. Preparation of nanocarbon hybrid (NCH)

Nanocarbon hybrid (NCH) was prepared according to the method reported previously (Shouman and Fathy, 2018) with some modifications. During the sol-gel process of resorcinol (R)-formaldehyde (F)-sodium dodecyl sulfate (SDS) precursors in the presence of sodium carbonate as a catalyst (C), 1 % (w/w) of CNTs were added. The molar ratios of the used reactants with respect to resorcinol were determined as; R/F = 0.5, R/C = 500, R/W = 0.027 and R/SDS = 9.36×10^{-6}. A 0.1 M sodium hydroxide solution was used to change the pH of the sol to 6.0. The obtained hydrogel was then transferred into ground-glass stopper flask and heated in a forced air-oven at 80 °C for 24 h to complete restoring and gelling process followed by further drying at 100 °C for another 48 h. After cooling, the obtained hybrid xerogel was carbonized at 350 °C for 1 hour, and then steadily increased to 850 °C at rate of 10 °C/min for 2 h under flowing of N_2 gas. To enhance the binding of metal on its surface, the obtained NCH was acidified with 30% hydrogen peroxide and refluxed at 60 °C for 2 h while stirring. The resulting sample was filtered, washed with hot distilled water, and then dried at 100 °C overnight.

2.3. Characterization of the prepared NCH

The morphology of the NCH (nanocarbon hybrid) was estimated deeply by high resolution-transmission electron microscopy (HR-TEM, JEM-1230, Japan). For distribution and identification of elemental composition on the surface of the prepared and treated NCH, Energy Dispersive X-ray analysis (EDX) was applied in combination with SEM analysis. Scanning Electron Microscopy-Energy Dispersive X-ray (SEM-EDX) is conducted with a FEI Quanta 250 equipped with a Bruker Si(Li) EDX detector. The surface functional groups of the produced NCH were determined by Fourier transform infrared spectroscopy (FTIR), using KBr pellets (JASCO, FT-IR-460 plus).

The specific surface area (S_{BET}, m^2/g) was determined using Brunauer- Emmett- Teller (BET) equation. The amount of nitrogen adsorbed at the relatively pressure of $p/p_0 = 0.96$ and -196 °C was employed to determine total pore volume (V_T, cm^3/g) and average pore diameter ($\bar{r}$, Å) (BEL-Sorp, Microtrac Bel Crop, Japan) (IUPAC, 1991). In addition, various textural parameters were analyzed and evaluated using α_s method such as total surface area (S_t^{α}, m^2/g), non-microporous surface area (S_n^{α}, m^2/g), and the micropore volume (V_m^{α}, cm^3/g) (Selles-Perez and Martin-Martinez, 1991). The pore size distributions (micro- and mesopores) were determined by means of the Nonlocal Density Functional Theory (NLDFT) (Ravikovitch and Neimark, 2002).

2.4. Determination of Fe, As, and Mn ions concentration

At the end of each experiment, the solution was filtered using a Whatman No. 42 filter paper and the metal ions concentrations were determined using ICP-OES according to APHA (2017). ICP-OES analysis is conducted using the Agilent 5100 Synchronous Vertical Dual View (SVDV) after calibration with a series of Fe, AS, and Mn calibration solutions. Linearity is guaranteed for a calibration range of 0.1 mg/l - 100 mg/l.

2.5. Quality control

All experiments were carried out in triplicate. Relative standard deviations (RSD) were less than 5 % in all experiments. The recovery was within the accepted range between 97 and 103 %.

2.6. Batch adsorption experiment

2.6.1. Effect of pH

To avoid metal ions precipitation due to pH impact, 2 mg/l of metal mixture solution was run without NCH for time intervals up to 120 min at room temperature (25 °C) and 120 rpm using thermostatic shaker at pH values of 2, 4 and 6. To determine the optimum pH value for the adsorption capacity of the prepared NCH, 50 ml of the metal mixture solution with initial concentration of 2 mg/l was incubated with NCH (0.05 g) at different pH values of 2, 4 and 6. The pH adjustment was done using a 0.01 M NaOH/HCl solutions and the pH value was measured using Thermo Scientific/Orion VERSASTAR advanced electrochemistry meter.

2.6.2. Effect of contact time

To study the effect of contact time on the adsorption of NCH, a set of 50 ml of metal mixture (Fe, As, Mn) solutions with concentration level of 2 mg/l were incubated with 0.05 g of CNH. The mixtures were agitated for 5, 10, 20, 30, 45, 60, 90 and 120 min at 120 rpm using thermostatic shaker at ambient temperature. The samples were filtered using Whatman filter paper No. 42 before ICP-OES measurements. When there was no further decrease in metal ions concentration, the equilibrium time for the mixture of metal ions was set.

2.6.3. Effect of sorbent dose

The effect of NCH dose was conducted using 50 ml of mixture of metal ions (Fe, As, and Mn) solution with initial level of 50 mg/l. The solutions were incubated with various carbon doses (0.01, 0.015, 0.025, 0.050 and 0.100 g) and agitated at 120 rpm using a thermostatic shaker at ambient temperature until equilibrium was reached.

The ability and maximal adsorption capacity for NCH were investigated using different initial metal ion concentrations (5–400 mg/l).

The adsorbent's removal efficiency (%R), equilibrium time (q_t) and uptake (q_e) were calculated using the following equations (Eqs. (1) and (2)):

$$\% R = [(C_o – C_e)/ C_o] \times 100 \quad (1)$$

$$q_t \text{ or } q_e = (C_o – C_e)\ V/m \quad (2)$$

Where, C_o and C_e are the initial and equilibrium concentration of metal ions (mg/l), V is the volume of solute solution (l), m is the weight of the adsorbent used (g).

2.7. Kinetics modeling

For simulating the kinetics of As, Fe, and Mn adsorption onto NCH, two widely used kinetics models, pseudo-first order and pseudo-second order were used. The equations of both models are expressed as Pseudo-fist order model (Lagergren, 1898):

$$\log(q_e - q_t) = \log q_e - \left[\frac{k_1}{2.303}\right] t \quad (3)$$

Pseudo-fist order model (Ho and Mckay, 1999):

$$\frac{t}{q_t} = \frac{1}{k_2 q_e^2} + \left[\frac{1}{q_e}\right] t \quad (4)$$

Where, q_e is the amount of adsorbed per unit gram of adsorbent (mg/g) at equilibrium, while q_t is the amount of adsorbed per unit gram of adsorbent (mg/g) at time t, k_1, and k_2 are the respective model constant on equilibrium time (t).

2.8. Adsorption isotherms

Many equilibrium models have been developed by altering the initial metal ions concentration from 2 to 400 mg/L while maintaining the other optimal operating conditions. The equilibrium data were described using the Langmuir, Freundlich, Temkin, and Dubinin–Radushkevich models.

2.9. Reusability of NCH

Desorption process is used to assess NCH's ability to regenerate as an adsorbent material for re-use under appropriate and cost-effective circumstances. In this study, NCH loaded with metal ions were transferred to a flask holding 100 mL of 0.5 M HCl as a desorbing agent. The mixture was shaken for 30 min at 120 rpm using a rotary shaker at ambient temperature. The mixture was then filtered, and the filtrate was analyzed for metal ions concentration. The eluted NCH were washed repeatedly with deionized water to remove any residual desorbing solution and then dried till reaching constant weight before another use. The adsorption–desorption cycle was repeated six times using the same NCH with an initial metal ions concentration of 50 mg/L each time. The following formula (Eq. 5) is used to compute the regeneration efficiency (RE%) of NCH as an adsorbent agent.

$$RE\% = (A_r/A_0) \times 100 \quad (5)$$

In the aforementioned equation, A_r and A_0 denote the adsorption capacity of the NCH after regeneration (mg/g) and the adsorption capacity of NCH before regeneration (original capacity) (mg/g), respectively (Sun et al., 2009).

3. Results and discussion

3.1. Characterization of sorbent agents

3.1.1. Morphological studies by TEM and SEM

The morphology of the prepared nanocarbon hybrid (NCH) using TEM tool is displayed in Figure 1a. The image reflects the formation of interconnected nodules in carbon xerogel matrix (CX) with average sizes ranged between 20 and 50 nm. In addition, multi-walled CNTs (MWCNTs) bundles along the network of CX can be observed as shown in Figure 1a. MWCNTs have outer diameters ranging from 22 to 66 nm. As shown in Figure 1b, the surface morphology of NCH revealed that CNTs are cross-linked with carbon nodules in CX network. Due to van der Waals forces, the diameter of MWCNTs is ranged between 10 and 100 nm and have a clear propensity to bundle together in ropes. This result is agreement with previous study conducted by Shouman and Fathy (2018).

3.1.2. FTIR spectrum

The adsorptive capacity of the activated carbons is influenced by their surface chemical structure. Carboxylic, phenolic, hydroxyl, carbonyl, and lactone groups are frequently suggested as surface functional groups on carbon surfaces (Girgis et al. 2009, 2012). The FTIR spectrum of the sample under investigation reveals the following fundamental surface functional groups: 1638 cm^{-1}, 1432 and 1386 cm^{-1}, 1088 cm^{-1}, and 467 cm^{-1}, 3430 cm^{-1}, 2926 cm^{-1}, and 2855 cm^{-1}, 1638 cm^{-1}, 1432 and 1386 cm^{-1}, 1088 cm^{-1}, and 467 cm^{-1}. These absorption bands referred to stretching vibration mode of O–H, C–H, C=C, C–O in ethers, esters, hydroxyls and phenol groups; as well as out-of-plane vibration of C–H moieties of aromatic structure, confirming the incorporation of CNTs into CX matrix (Shouman and Fathy, 2018; Fathy et al., 2019). To explore the surface adsorption efficiency of NCH, FTIR spectrum for NCH after adsorption is reported also. It is found that all oxygen-containing functional groups disappeared as a result of interactions between these groups and adsorbed metals. Thereof, such oxygen-containing functional groups have a high impact on the uptake of metal ions, confirming the high adsorptive behavior of NCH towards removal of studied heavy metals.

The EDX analysis of NCH before and after the adsorption process (Figure 2 a, b) revealed that carbon makes up the vast bulk of NCH,

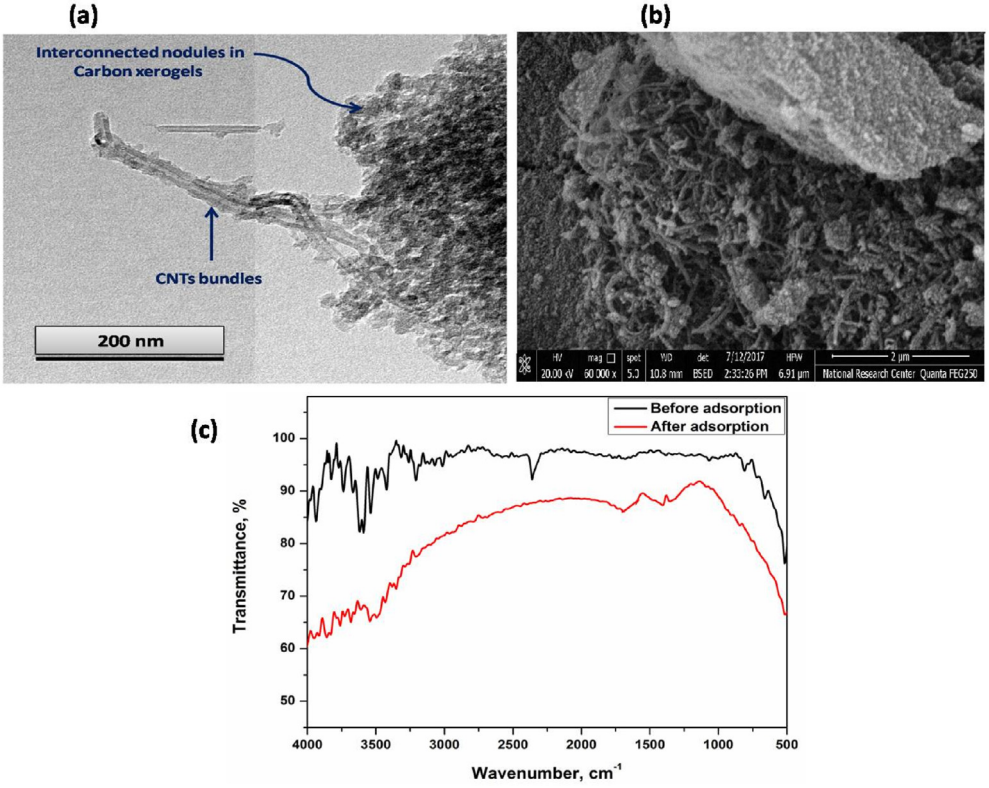

Figure 1. (a) TEM image and (b) SEM image and (c) FTIR spectrum of nanocarbon hybrid sample before and after adsorption.

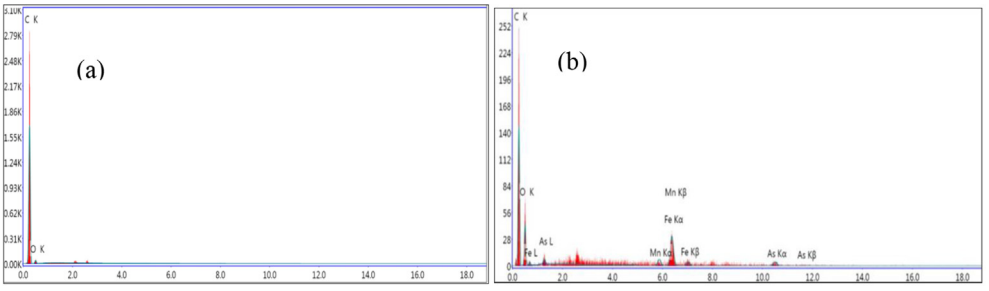

	(a) NCH before adsorption		(b) NCH after adsorption				
Element	C	O	C	O	Fe	As	Mn
Wt. %	91.45	8.55	58.45	19.04	10.85	9.82	1.84
At. %	93.44	6.56	75.85	18.55	3.03	2.04	0.52

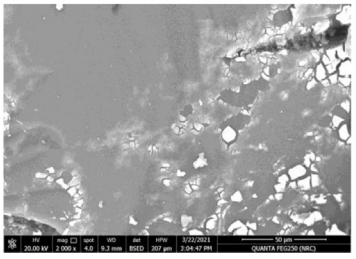

Figure 2. EDX spectrum of (a) NCH, (b) NCH after adsorption of metal ions and SEM image for NCH after metal ion adsorption (c).

accounting for 91 % and 58 % (weight percent) for both, respectively. Referring to Figure 2b, the NCH after metal ions adsorption, the carbon content is reduced by 33 %, whereas the weight percent of oxygen is enhanced from 9 to 19 % after adsorption process; whereas, Fe, As, and Mn constituted about 11 %, 10%, and 2 % of the total, respectively according to EDX results as shown in Figure 2b. Referring to Figure 2c, the white spots observed on the surface of NCH following a metal adsorption experiment can be attributed to metal ions adsorption, which is also verified by the EDX spectrum (Figure 2b) confirming the surface adsorption of metal ions through physisorption process.

3.1.3. Analysis of porous texture

The N_2 adsorption–desorption isotherm of NCH sample is shown in Figure 3a. This illustration shows a type-I isotherm, which indicates the presence of a well-developed microporous structure according to the IUPAC classification. This finding is supported by the NLDFT pore size distribution curve (Figure 3b), which shows a uniform model distribution with a maximum pore width of 1.50 nm. In addition, the isotherm has an H3 type hysteresis loop shape, which corresponds to the presence of narrow mesopores. Table 1 summarizes the measured porous parameters, revealing that the total specific surface area, total pore volume and mean pore diameter are 162 m^2/g, 0.129 cm^3/g and 3.2 nm, respectively. The sample had an average of microporosity of 87.5 %. Such porous characteristics promote the adsorption capacity of NCH to uptake of metal ions as seen in the following adsorption results.

3.2. Adsorption mechanism

3.2.1. Effect of pH

The pH of a solution reflects the concentration of protons in the solution, which is a very influential parameter in controlling metal adsorption. Heavy metal adsorption on NCH is strongly dependent on solution pH as many forms of metal ion species (e.g. Mn^+, $M(OH)_n$, $M(OH)^+_{n-1}$) would be present in the solution as a function of solution pH due to hydrolysis (Xu et al., 2008). A preliminary experiment was conducted without NCH at pH (2, 4, and 6) to confirm that the removal of metal ions didn't depend on precipitation, the results showed that no precipitation occurred at the investigated pH. The removal percentages for the metal ions were very low at pH 2 when NCH was added as described in detail in the adsorption experiments. At pH 4, the removal percentage for Fe ions increased dramatically and reached 95%, but it remained low for As and Mn ions. The maximal removal occurred at pH 6 and was recorded as 40%, 97%, and 45% for As, Fe, and Mn, respectively (Figure 4). When the pH is low, more protons can exchange with heavy metal cations (Yang et al., 2019), and the high concentration of H^+ can protonate the surface functional groups (e.g. ^-OH) of carbon, resulting in an increase in the number of surface positive charges (Ma et al. 2018, 2019). The adsorption of heavy metals would be reduced as the protonation increased due to the electrostatic repulsion (Wang et al., 2014). On the other hand, at high pH, the negative surface charge creates electrostatic interactions that are favorable for cation ion adsorption (Ren et al., 2011; Sayed et al., 2019). Arsenic in natural waters is mainly found with its inorganic forms of As(III) (H_3AsO_3) and/or As(V) (arsenic oxyanions such as H_3AsO_4, H_2AsO^{4-} and $HAsO_3^{2-}$) depending on the pH medium. As (III) is more toxic and harder to be adsorbed than As (V) on a solid surface and thus it can be converted to As (V) by aiding oxidizing agents. The present NCH with its oxygen surface functional groups could convert As (III) to As (V) forms and adsorb them at pH 6 (Tolkou et al., 2020). For Mn adsorption, A partial hydrolysis of Mn(II) ions with increasing pH from 4 to 6, forming complexes with OH^- such as $Mn(OH)^+$, $Mn(OH)_2$, $Mn_2(OH)^+_3$, Mn_2OH^{3+}, and $Mn(OH)_4^{2-}$ species in solution was happened (Omri and Benzina, 2012). The formation of As oxyanions and Mn hydroxides at pH 6 may explain why their removal is less than Fe removal by NCH.

3.2.2. Effect on contact time

Adsorption equilibrium between the adsorbent (NCH) and adsorbate (metal ions) should be achieved to ensure that the adsorption process is completed. The equilibrium time is attained when there is no more adsorption of metal ions onto the adsorbent agent. Figure 5 shows the effect of contact time on the adsorption of As, Fe, and Mn using NCH. For 120 min, the adsorption capabilities of a mixture of As, Fe, and Mn (2 mg/L each) were investigated. Within 10 min, the adsorption capacity was hastily improved, and the removal percentages for As, Fe, and Mn were 30 %, 97 %, and 41 %, respectively. The maximum adsorption for Fe (97.0%) and Mn (44.5%) was attained in 30 min; however, the removal percentage for As reached 33 % in 30 min, raised to 40 % after 60 min, and then declined to 30 % within 90 and 120 min (Figure 5). The adsorption of the metal ions mixture onto the NCH occurred easily and rapidly at the beginning of the contact (stage 1), followed by a second, more slowly adsorption stage, according to the data showed in Figure 5. The adsorption attained equilibrium in the third stage when the amount of metal ions adsorbed onto the NCH equaled the amount of metal ions desorbing from the NCH. The rapid adsorption at the initial stage is due to the availability of huge number of adsorptive sites (El-Kady et al., 2016; Egbosiuba et al., 2020) and a high external diffusion rate of metal ions (Doulia et al., 2009). Adsorption transfer from extra diffusion to internal diffusion was blamed for the subsequent delayed adsorption in the second stage, while the saturated adsorption stage is due to the electrostatic repulsion between metal ions and the adsorbent, which limits the function of the remaining activated sites (Doulia et al., 2009; Shi et al., 2009). As a result, the equilibrium time to reach the maximum adsorption capacity (q_{max}) was achieved in less than 30 min.

3.2.3. Effect of NCH dose

The effectiveness of NCH in removing multi-metal ions (As, Fe, Mn) is shown in Figure 6. It is observed that increasing the NCH dose from 0.01 g to 0.05 g/50 mL solution significantly increases the removal percentages for Fe from 40% using 0.01 g of NCH to 71 and 80% with doses of 0.025 and 0.05 g, respectively. The same trend was observed for Mn, with an increasing rate of 18% when the dose of NCH was increased from 0.01 to 0.025 g and again from 0.025 g to 0.05 g. The removal percentage for Mn was increased by one-third to 40% by increasing the dose to 0.1 g;

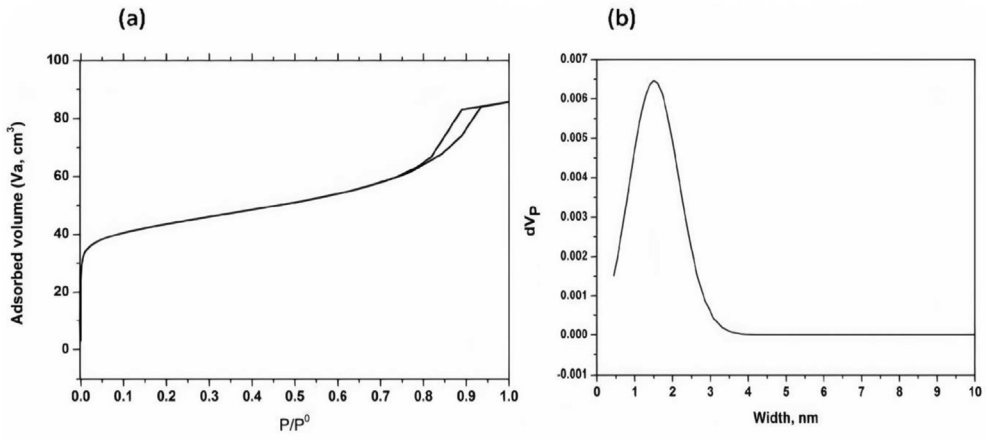

Figure 3. (a) Nitrogen adsorption-desorption isotherm and (b) NLDFT pore size distributions curve of the prepared nanocarbon hybrid sample.

Table 1. Porous properties of the prepared sample.

Samples	S_{BET} (m^2/g)	V_T (cm^3/g)	$\bar{r}$ (Å)	S^{α}_t (m^2/g)	S^{α}_n (m^2/g)	S^{α}_{mic} (m^2/g)	V^{α}_m (cm^3/g)	$S^{\alpha}_{mic}/S^{\alpha}_t$ %	Maximal pore width (nm)
NCH	162	0.129	32	174	22	152	0.085	87.5	1.50

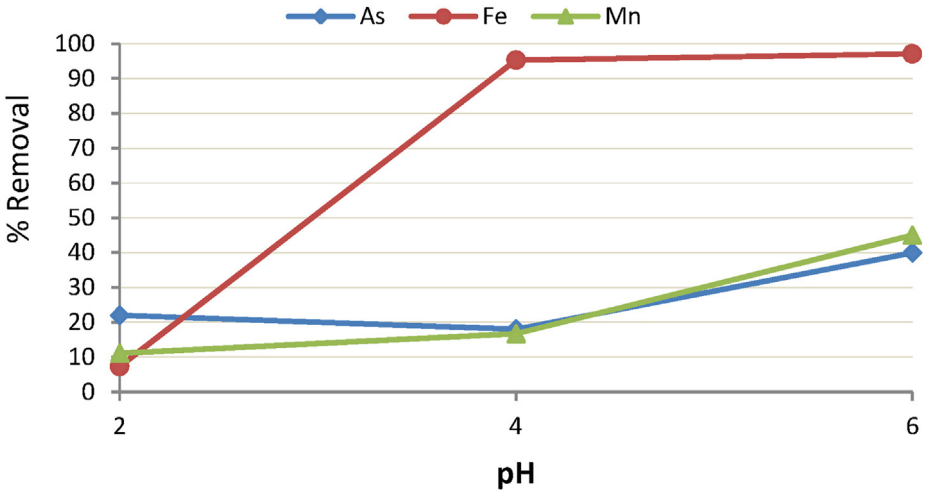

Figure 4. Effect of pH on the adsorption capacity of metal ions (As, Fe, Mn) onto NCH (Experimental conditions: adsorbent: 0.05 g, metal ion concentration: 2 mg/l, solution: 50 ml, T: 25 °C, agitation speed: 120 rpm).

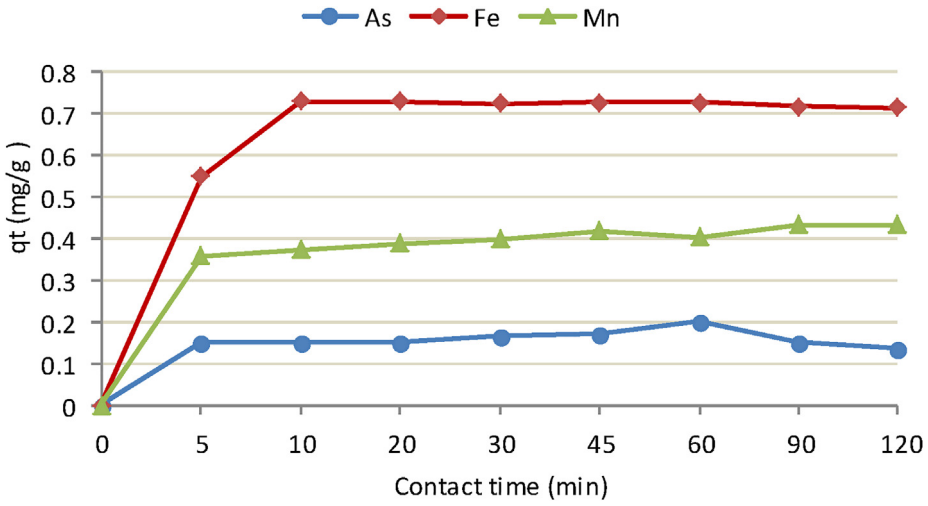

Figure 5. Effect of contact time on the adsorption capacity of metal ions (As, Fe, Mn) onto NCH (Experimental conditions: adsorbent: 0.1 g, metal ion concentration: 2 mg/l, solution: 50 ml, pH: 6.0, T: 25 °C, agitation speed: 120 rpm).

however, a 3% decrease was observed when increasing the dose of NCH to 0.1 g for Fe. However, no significant changes has been observed in case of arsenic as the removal percentages recorded 30 %, 29 %, 36 %, and 31% with dosages of 0.01, 0.025, 0.05, and 0.1 g, respectively.

There is a definite trend toward increased removal effectiveness by raising the dose up to 0.05 g/50 ml solution for Mn and Fe, which is linked to the availability of more adsorption sites (Jun et al., 2019). The adsorption percentage was reduced by raising the dose to 0.1 g. Two variables can explain the decrease in removal percentage with an increase in adsorbent dosage. First, an increase in adsorbent dosage at a constant adsorbate concentration and solution volume causes instauration of adsorption sites, and second, particle aggregation caused by high adsorbent mass reduces adsorption capacity. As a result of this aggregation, the adsorbent's overall surface area decreases, consequently the active sites available for binding were decreased (Oladoja and Akinlabi, 2009).

3.3. Kinetics modeling

Adsorption kinetics of As, Fe, and Mn ions upon NCH surface were investigated by pseudo-first-order and pseudo-second-order kinetics which are illustrated in Eqs. (3) and (4). The linear pseudo first and second order plots at room temperature are obtained by plotting log (qe-qt) versus t (Figure 7a) and t/qt versus t (Figure 7b), respectively from which the kinetic parameters values of k_1, q_e and k_2 are calculated and presented in Table (2). The R^2 values of the pseudo-first-order model for As, Fe and Mn ions are (0.028, 0.128 and 0.247, respectively), indicating that this model was unsuitable to represent the kinetic profile because of the apparent lack of linear correlation. However, the situation was significantly different for the pseudo-second-order model, where the kinetic plots have appropriate linearity as evidenced by R^2 values close to 1.0 (0.98, 0.99 and 0.99) for As, Fe and Mn ions, respectively. Moreover, the values of q_e values calculated from pseudo-second-order equation for

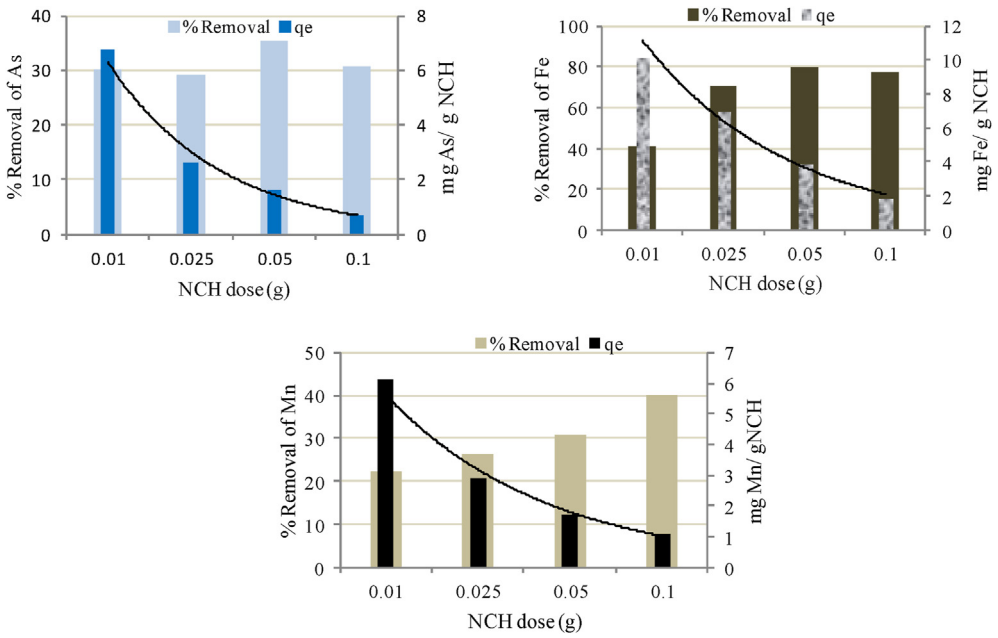

Figure 6. Effect of NCH dose on the adsorption capacity of metal ions (As, Fe, Mn) (Experimental conditions: metal ion concentration: 5 mg/l, solution: 50 ml, pH: 6.0, T: 25 °C, contact time: 30 min, agitation speed: 120 rpm).

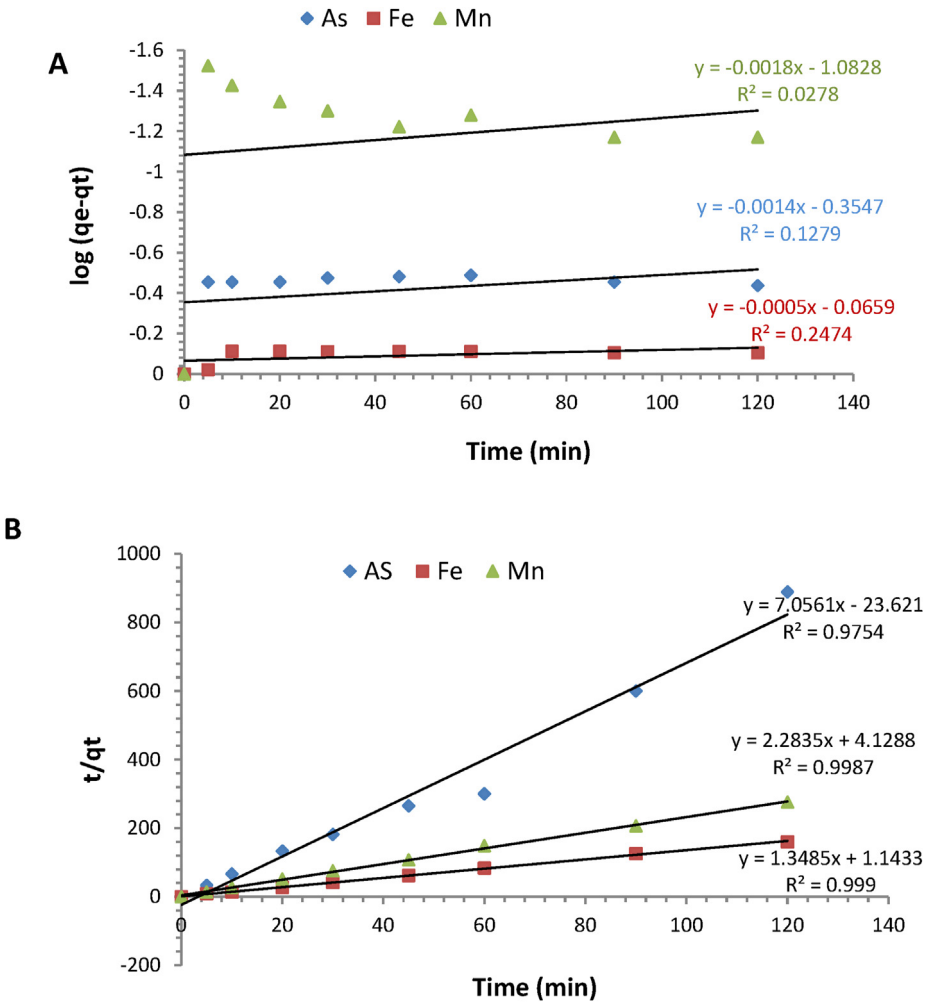

Figure 7. (A) Pseudo-first-order and (B) Pseudo-second-order kinetic models for adsorption of As, Fe and Mn ions on NCH surface.

As, Fe and Mn ions were (0.14, 0.73 and 0.43 mg/g) respectively which is very near to the experimental value of q_e (0.125, 0.718 and 0.382 mg/g), respectively. On the other hand q_e values estimated through the pseudo-first order kinetics (0.7, 0.94 and 0.34 mg/g), respectively were far from that estimated experimentally. These results revealed that the adsorption of As, Fe and Mn onto NCH could be best described by the pseudo second-order kinetic model (see Table 2).

Table 2. Kinetic models parameters for adsorption of As, Fe and Mn ions on NCH.

	Pseudo-first-order			Pseudo-second-order		
	q_e (mg/g)	k_1	R^2	q_e (mg/g)	k_2	R^2
As	0.70	-0.0032	0.13	0.14	-2.108	0.98
Fe	0.94	-0.0012	0.25	0.74	1.591	0.99
Mn	0.34	-0.0041	0.028	0.43	1.263	0.99

3.4. Adsorption isotherm models

The adsorption isotherms of Langmuir, Freundlich, Temkin, and Dubinin–Kaganer–Radushkevich (DKR) are commonly employed to elucidate the mechanism of metal ion adsorption on the produced NCH (Langmuir, 1916; Freundlich, 1906; Dubinin and Radushkevich, 1947; Temkin and Pyzhev, 1940).

3.4.1. Langmuir isotherm model

The Linear and simplified form of Langmuir equation is given by Eq. (6):

$$\frac{C_e}{Q_e} = \frac{1}{Q_{maxK_1}} + \frac{C_e}{Q_{max}} \tag{6}$$

Where Q_e (mg/g) is the amount adsorbed at equilibrium, C_e (mg/l) is the equilibrium metal ion concentration in aqueous solution, K_L (L^{-1}) is the Langmuir constant which related to the adsorption energy where, K_l and Q_{max} are Langmuir constants related to sorption energy and sorption capacity, respectively. K represents enthalpy of adsorption and should vary with temperature. Q_{max} is the maximum adsorption capacity of metal ions per unit mass of sorbent when all binding sites are occupied. Where, monolayer adsorption onto the surface with a finite number of identical sites is the hypothesis of Langmuir isotherm (Langmuir, 1916). The results showed a linear plot obtained from C_e/Q_e vs. C_e confirming that the adsorption of Fe, Mn and As ions metals doesn't follow the Langmuir model (Figure 8).

3.4.2. Freundlich isotherm model

The Simplified Freundlich equation is given by Eq. (7)

$$lnQ_e = lnK_f + \frac{1}{n} lnC_e \tag{7}$$

Where k_f and n are the Freundlich constants and are related to the sorption capacity of the NCH and its intensity (Freundlich, 1906). Equilibrium data are the essential aspect in deciding between Langmuir and Freundlich isotherms. The Langmuir and Freundlich isotherm parameters are presented in Table 3. For metal ion adsorption, the Freundlich isotherm provides a better fit than the Langmuir model, with R^2 values of 0.962, 0.958, and 0.951 for Mn, As, and Fe ions, respectively, demonstrating the Freundlich model's excellent adaptability to the sorption of the studied metal ions onto NCH adsorbent (Figure 9). Metal ion adsorption on NCH is expected to be monolayer and multilayer.

3.4.3. Dubinin–Radushkevich isotherm model

It's an extended model because it doesn't assume a uniform surface or a constant sorption potential; it provides information on sorbent porosity as well as adsorption energy. The adsorption energy value can be used to determine whether the adsorption process is physical or chemical (Dubinin and Radushkevich, 1947; Abdelwahab et al., 2015). The linear equation of DKR isotherm can be simplified to the following Eq. (8)

$$q_{e=\ q_m exp^{-}\beta\varepsilon 2} \tag{8}$$

Where q_e is the number of metal ions adsorbed per unit weight of adsorbent (mol/g), q_m is the maximum sorption capacity, b is the activity coefficient related to mean sorption energy, and Ɛ is the Polanyi potential, which is equal to:

$$\varepsilon = RTln\left(1 + {}^{1}/_{C_e}\right) \tag{9}$$

Where R is the gas constant (kJ/mol K) and T is the temperature (K). By plotting a relationship between lnq_e and ε^2 as shown in Figure 10, β and q_{DR} can be obtained. (D-R) isotherm parameter β used to determine adsorption energy E (KJ/mol) as given in the following Eq. (10):

$$E = \frac{1}{\sqrt{-2\beta}} \tag{10}$$

Fe, Mn, and As ions have adsorption energies of 4.08, 1.95, and 2.42 kJ/mol, respectively. The positive values of E indicated that the adsorption of the metal ions onto the NCH is endothermic. When the E value ranged between 8 and 16 kJ/mol, the adsorption process is chemical in nature (Samadi et al., 2015). In our study, the value of E is found to be less than 8 kJ/mol, indicating that the sorption process is physical adsorption.

3.4.4. Temkin isotherm model

The interactions between adsorbents and adsorbates were defined by the Temkin isotherm (Figure 11). Due to adsorbent-adsorbate interactions,

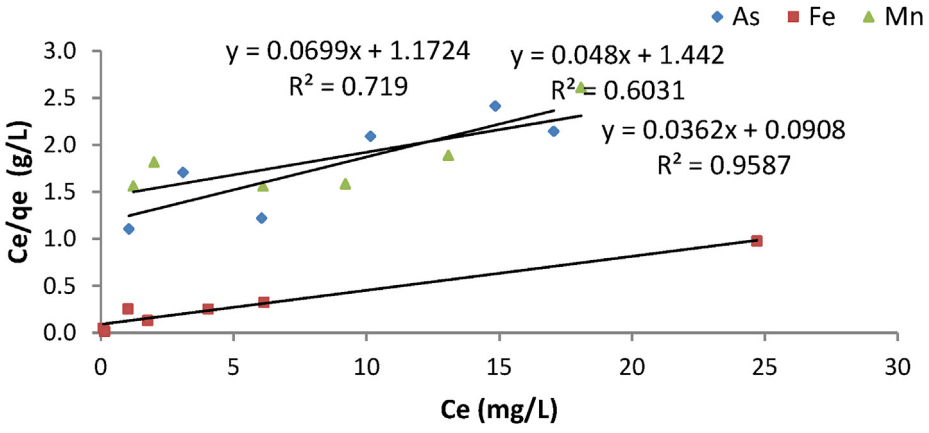

Figure 8. Langmuir isotherm for (Fe, Mn and As) ions adsorption onto NCH.

Table 3. Summary of isotherm models parameters for metal ions adsorption on NCH.

	Langmuir model			Freundlich model			Dubinin–Kaganer–Radushkevich (DKR)			
	K L/mg	q_{max} (mg/g)	R^2	K_f	n	R^2	Xm (mol/g)	β (mol^2/j^2)	E, KJ/mol	R^2
As	0.038	20	0.822	0.84	1.23	0.969	0.297	7.74×10^{-8}	2.54	0.817
Fe	0.136	48.08	0.958	8.52	1.75	0.99	1.23	2.0×10^{-8}	4.08	0.7
Mn	0.033	20.83	0.603	0.2	0.72	0.972	0.48	1.17×10^{-7}	1.95	0.838

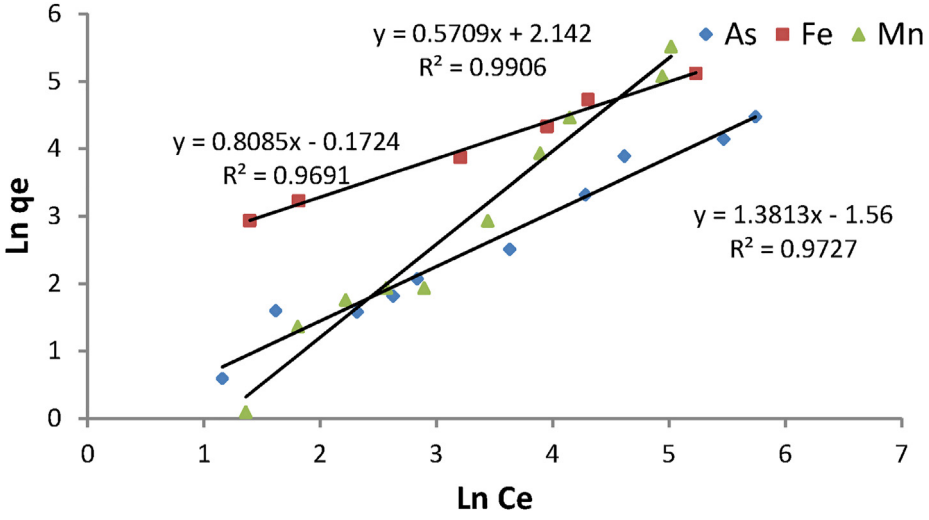

Figure 9. Freundlich isotherm for (Fe, Mn and As) ions adsorption onto NCH.

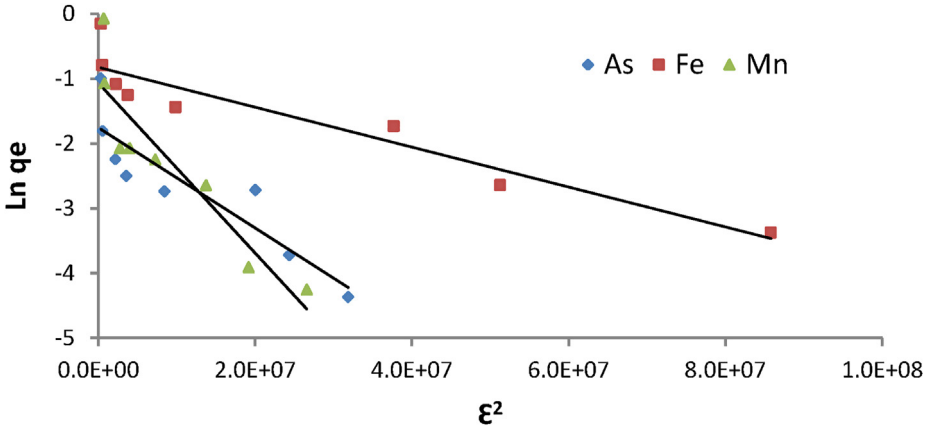

Figure 10. DKR sorption isotherm of metal ions (As, Fe, Mn) adsorption onto NCH.

it is assumed that the adsorption energy reduces linearly with surface coverage. The following equation (Eq. 11) gives the linear version of the Temkin isotherm model (Temkin and Pyzhev, 1940):

$$q_e = B_T \text{ In } K_T + B_T \text{ In } C_e \quad (11)$$

Where $B_T = RT/b$ is constant related to heat of sorption (J/mol), T is the absolute temperature (K), R is the ideal gas constant (8.314 J/mol), b is a constant related to the heat of sorption (J/mol) and K_T is the Temkin isotherm constant (l/g).

3.5. Adsorption/desorption process for metal ions uptake by NCH

Stability is a significant factor when the same sorbent material is used in multiple adsorptions and desorption cycles. Figure 12 shows the regeneration efficiency (RE %) and adsorption capacity (qe, mg metal ion/g NCH) of NCH as an adsorbent agent. The regeneration effectiveness (RE %) of the NCH for As and Mn is marginally reduced after the first regeneration cycle, reaching 96.6 % and 89.0 %, respectively. However, following the second cycle, the RE % for both As and Mn dropped by 10% and 14%, respectively, to 86 % and 75 %. After cycle 6, As and Mn had a RE of 67 % and 62 %, respectively. Since the RE percent for all 6 cycles was greater than 99 percent, NCH's regeneration efficiency for Fe can be described as stable. The dominance of As and Mn at adsorption sites hampered the adsorption of fresh As and Mn, resulting in a 30% and 40 % reduction in regeneration efficiency and adsorption capacity after the cycle 6, respectively. Even after 6 cycle generations, the adsorption and desorption data demonstrated that NCH had outstanding regeneration and reusability toward the mixture of metals studied, especially iron.

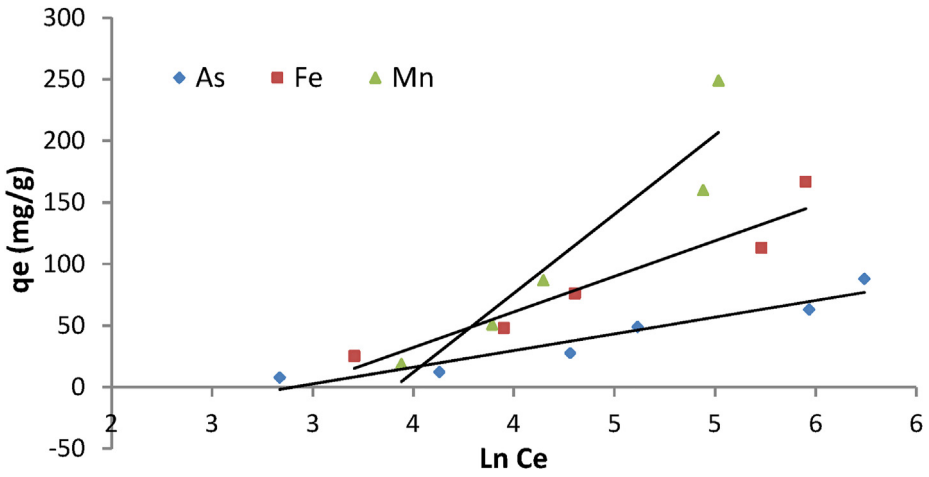

Figure 11. Temkin plot of metal ions (Fe, Mn and As) adsorption on NCH.

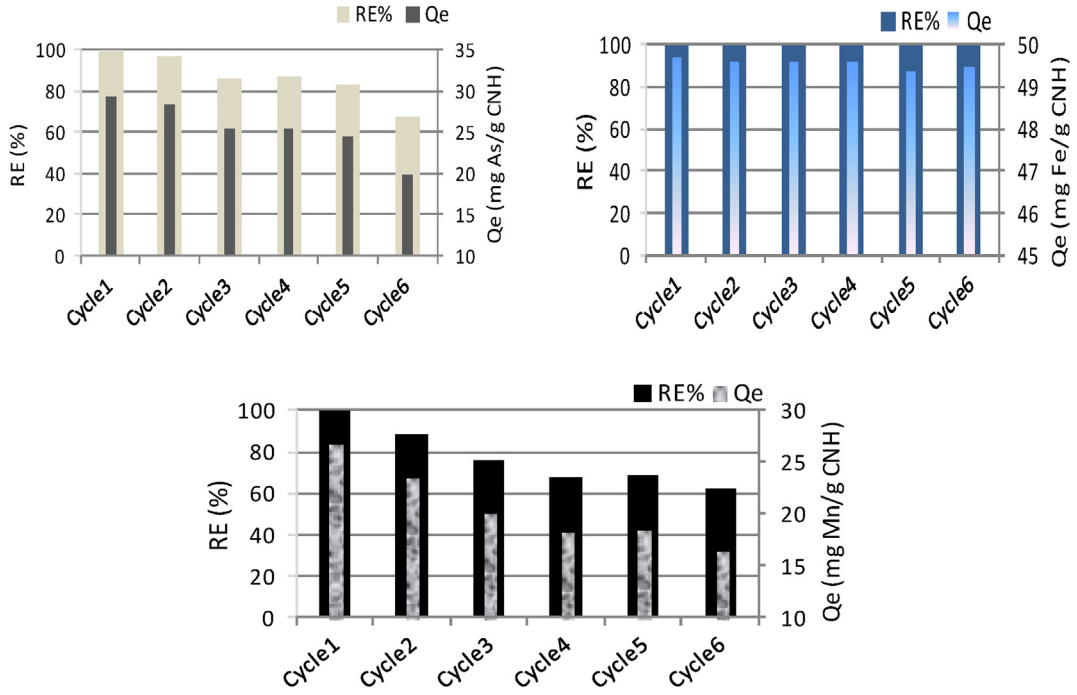

Figure 12. Regeneration efficiency and adsorption capacity of NCH against the mixture of As, Fe, and Mn.

4. Conclusion

In this work, the prepared nanocarbon hybrid obtained from combination of carbon xerogels and carbon nanotubes exhibited high tendency to remove toxic metals such as As, Mn and Fe ions. The maximum removal was achieved within 30 min, according to batch adsorption kinetic experiments. For Mn and Fe, there is a clear trend toward enhanced removal efficacy when the dose is increased to 0.05 g/50 ml solution, which is connected to the availability of more adsorption sites. By increasing the dose to 0.1 g, the adsorption % was lowered. The results showed that Freundlich isotherm fitted the adsorption processes with regression coefficient $R^2 > 0.969$, 0.99 and 0.97 for As, Fe and Mn ions, respectively. As well the adsorption energy (E), obtained from D–R isotherm, confirming that the adsorption proceed via physical adsorption. NCH exhibited satisfactory adsorption efficiencies (q_{max}) of 20, 20.83 and 48.08 mg/g for As, Mn and Fe ions, respectively. The adsorption and desorption results showed that NCH had excellent regeneration and reusability toward the mixture of AS, Mn, and Fe even after 6 cycle generations. Consequently, it was concluded that NCH was a promising adsorbent for rapid simultaneous removal of mixture of metal ions from aqueous medium.

Declarations

Author contribution statement

Mohamed A. Embaby: Conceived and designed the experiments; performed the experiments; Analyzed and interpreted the data; Wrote the paper.

Shimaa M. Abdel Moniem: Analyzed and interpreted the data.

Nady A. Fathy: Analyzed and interpreted the data; Contributed reagents, materials, analysis tools or data; Wrote the paper.

Ahmed A. El-kady: Designed the experiments; Performed the experiments; Analyzed and interpreted the data; Wrote the paper.

Funding statement

This research did not receive any specific grant from funding agencies in the public, commercial, or not-for-profit sectors.

Data availability statement

Data will be made available on request.

Declaration of interests statement

The authors declare no conflict of interest.

Additional information

No additional information is available for this paper.

References

Abdelwahab, O., Fouad, Y.O., Amin, N.K., Mandor, H., 2015. Kinetic and thermodynamic aspects of cadmium adsorption onto raw and activated guava (*Psidium guajava*) leaves. Environ. Prog. Sustain. 34, 351–358.

APHA, 2017. Standard Method for Water and Wastewater, 23rd edition.

Bohli, T., Ouederni, A., Villaescusa, I., 2017. Simultaneous adsorption behavior of heavy metals onto microporous olive stones activated carbon: analysis of metal interactions. Euro-Mediterr. J. Environ. Integr. 2, 19.

Carolin, C.F., Kumar, P.S., Saravanan, A., Joshiba, G.J., Naushad, M., 2017. Efficient techniques for the removal of toxic heavy metals from aquatic environment: a review. J. Environ. Chem. Eng. 5 (3), 2782–2799.

Doulia, D., Leodopoulos, Ch., Gimouhopoulos, K., Rigas, F., 2009. Adsorption of humic acid on acid-activated Greek bentonite. J. Colloid Interface Sci. 340 (2), 131–141.

Dubinin, M.M., Radushkevich, L.V., 1947. Equation of the characteristics curve of activated charcoal. Chem. Zent. 1, 875.

Egbosiuba, T.C., Abdulkareem, A.S., Kovo, A.S., Afolabi, E.A., Tijani, J.O., Roos, W.D., 2020. Enhanced adsorption of As(V) and Mn(VII) from industrial wastewater using multi-walled carbon nanotubes and carboxylated multi-walled carbon nanotubes. Chemosphere 254, 126780.

El Alfy, M., Merkel, B., 2010. Assessment of human impact on quaternary aquifers of Rafah Area, NE Sinai, Egypt. Int. J. Econ. & Environ. Geol. 1, 1–9.

El Alfy, M., 2013. Hydrochemical modeling and assessment of groundwater contamination in Northwest Sinai, Egypt. Water Environ. Res. 85, 211–223.

El-Kady, A.A., Abdel-Wahhab, M.A., 2018. Occurrence of trace metals in foodstuffs and their health impact. Trends Food Sci. Technol. 75, 36–45.

El-Kady, A.A., Sharaf, H.A., Abou-Donia, M.A., Abbès, Samir, Ben Salah-Abbès, Jalila, Naguib, M.N., Oueslati, Ridha, Abdel-Wahhab, M.A., 2009. Adsorption of Cd^{2+} ions on an Egyptian montmorillonite and toxicological effects in rats. J. Appl. Clay Sci. 44, 59–66.

El-Kady, A.A., Carleer, R., Yperman, J., D'Haen, J., Abdel-Ghafar, H.H., 2016. Kinetic and Adsorption study of Pb(II) towards different treated activated carbons derived from olive cake wastes. Desalin. Water Treat. 57 (18), 8561–8574.

Embaby, M.A., Ghafar, H.H.A., Shakdofa, M.M.E., Khalil, N.M., Radwan, E.K., 2017. Removal of iron and manganese from aqueous solution using some clay minerals collected from Saudi Arabia. Desalin. Water Treat. 65, 259–266.

EPA, 2018. 2018 Edition of the Drinking Water Standards and Health Advisories. EPA 822-F-18-001. Office of Water U.S. Environmental Protection Agency, Washington, DC.

European Union, 1998. Richtlinie 98/83/EG des Rates.

Fang, L., Li, L., Qu, Z., Xu, H., Xu, J., Yan, N., 2018. A novel method for the sequential removal and separation of multiple heavy metals from wastewater. J. Hazard Mater. 342, 617–624.

Fathy, N.A., El-Khouly, S.M., Aboelenin, R.M., 2019. Carbon xerogel/carbon nanotubes nanohybrid doped with Ti for removal of methylene blue dye. Egypt. J. Chem. 62, 2277–2288.

Fathy, N.A., 2017. Carbon nanotubes synthesis using carbonization of pretreated rice straw through chemical vapor deposition of camphor. RSC Adv. 7 (45), 28535–28541.

FPTCDW, 2016. Federal-provincial-territorial committee on drinking water, manganese in drinking water. https://www.canada.ca/en/health-canada/programs/consultation-manganese-drinking-water/manganese-drinking-water.html. (Accessed 27 March 2021).

Freundlich, H., 1906. Über die adsorption in lösungen. (Over the adsorption in solutions). Z. Phys. Chem. 57, 385–470.

Girgis, B.S., El-kady, A.A., Attia, A.A., Fathy, N.A., Abdel-Wahhab, M.A., 2009. Impact of air convection on H_3PO_4 activated biomass for Sequestration of Cu (II) and Cd (II) ions. Carbon Lett. 10 (2), 114–122.

Girgis, B.S., Attia, A.A., Fathy, N.A., 2011. Potential of nano-carbon xerogels in the remediation of dye-contaminated water discharges. Desalination 265, 169–176.

Girgis, B.S., El-Sherif, I.Y., Attia, A.A., Fathy, N.A., 2012. Textural and adsorption characteristics of carbon xerogel adsorbents for removal of Cu (II) ions from aqueous solution. J. Non-Cryst. Solids 358, 741–747.

He, S., Li, Y., Weng, L., Wang, J., He, J., Liu, Y., Zhang, K., Wu, Q., Zhang, Y., Zhang, Z., 2018. Competitive adsorption of Cd^{2+}, Pb^{2+} and Ni^{2+} onto Fe^{3+}-modified argillaceous limestone: influence of pH, ionic strength and natural organic matters. Sci. Total Environ. 637–638, 69–78.

Ho, Y.S., Mckay, G., 1999. Pseudo-second order model for sorption processes. Process Biochem. 34, 451–465.

Ibrahim, H.S., El-Kady, A.A., Ammar, N.S., Meesuk, L., Wathanakul, P., Abdel-Wahhab, M.A., 2013. Application of isotherm and kinetic models for the removal of lead ions from aqueous solutions. J. Environ. Eng. 139 (3), 349–357.

Igiri, B.E., Okoduwa, S.I.R., Idoko, G.O., Akabuogu, E.P., Adeyi, A.O., Ejiogu, I.K., 2018. Toxicity and bioremediation of heavy metals contaminated ecosystem from tannery wastewater: a review. Toxicity and bioremediation of heavy metals contaminated ecosystem from tannery wastewater: a review. J. Toxicol. 2568038.

Ihsanullah, Abbas A., Al-Amer, A.M., Laoui, T., Al-Marri, M.J., Nasser, M.S., Khraisheh, M., Atieh, M.A., 2016. Heavy metal removal from aqueous solution by advanced carbon nanotubes: critical review of adsorption applications. Separ. Purif. Technol. 157, 141–161.

International Agency for Research on Cancer (IARC), 2012. A review of human carcinogens. c. metals, arsenic, fibres and dusts. IARC (Int. Agency Res. Cancer) Monogr. Eval. Carcinog. Risks Hum. 100 (C).

Jun, B.M., Kim, S., Kim, Y., Her, N., Heo, J., Han, J., Jang, M., Park, C.M., Yoon, Y., 2019. Comprehensive evaluation on removal of lead by graphene oxide and metal organic framework. Chemosphere 231, 82–92.

Kumasaka, M.Y., Yamanoshita, O., Shimizu, S., Ohnuma, S., Furuta, A., Yajima, I., Nizam, S., Khalequzzaman, M., Shekhar, H.U., Nakajima, T., Kato, M., 2013. Enhanced carcinogenicity by coexposure to arsenic and iron and a novel remediation system for the elements in well drinking water. Arch. Toxicol. 87, 439–447.

Kwakye, G.F., Paoliello, M.M.B., Mukhopadhyay, S., Bowman, A.B., Aschner, M., 2015. Manganese-Induced Parkinsonism and Parkinson's disease: shared and distinguishable features. Int. J. Environ. Res. Publ. Health 12 (7), 7519–7540.

Lagergren, S., 1898. About the theory of so-called adsorption of soluble substances. Kungliga Svenska Vetenskapsakademiens 24, 1–39.

Langmuir, I., 1916. The constitution and fundamental properties of solids and liquids. J. Am. Chem. Soc. 38, 2221–2295.

Lingamdinne, L.P., Koduru, J.R., Roh, H., Choi, Y.-L., Chang, Y.-Y., Yang, J.-K., 2016. Adsorption removal of Co(II) from waste-water using graphene oxide. Hydrometallurgy 165, 90–96.

Liu, Y., Yan, J., Yuan, D., Li, Q., Wu, X., 2013. The study of lead removal from aqueous solution using an electrochemical method with a stainless steel net electrode coated with single wall carbon nanotubes. Chem. Eng. J. 218, 81–88.

Liu, X., Xu, X., Dong, X., Park, J., 2020. Competitive adsorption of heavy metal ions from aqueous solutions onto activated carbon and agricultural waste materials. Pol. J. Environ. Stud. 29 (1), 749–761.

Lotfi, S., Chakit, M., Belghyti, D., 2020. Groundwater quality and pollution index for heavy metals in Saïs plain, Morocco. J. Health Pollut. 10 (26), 200603.

Lu, J.-H., Yu, H.-S., Lee, C.-H., 2020. Chapter 11 - arsenic skin carcinogenesis: a prototypic model of chemical carcinogenesis featured with abnormal differentiation and aberrant immune responses. In: Prasad, Ananda S., Brewer, George J. (Eds.), Essential and Toxic Trace Elements and Vitamins in Human Health. Academic Press, pp. 165–170, 2020.

Ma, Y.-X., Shao, W.-J., Sun, W., Kou, Y.-L., Li, X., Yang, H.-P., 2018. One-step fabrication of β-cyclodextrin modified magnetic graphene oxide nanohybrids for adsorption of Pb(II), Cu(II) and methylene blue in aqueous solutions. Appl. Surf. Sci. 459, 544–553.

Ma, H., Yang, J., Gao, X., Liu, Z., Liu, X., Xu, Z., 2019. Removal of chromium (VI) from water by porous carbon derived from corn straw: influencing factors, regeneration and mechanism. J. Hazard Mater. 369, 550–560.

Malakootian, M., Mohammadi, A., Faraji, M., 2020. Investigation of physicochemical parameters in drinking water resources and health risk assessment: a case study in NW Iran. Environ. Earth Sci. 79, 195.

Montazer-Rahmati, M.M., Rabbani, P., Abdolali, A., Keshtkar, A.R., 2011. Kinetics and equilibrium studies on biosorption of cadmium, lead, and nickel ions from aqueous solutions by intact and chemically modified brown algae. J. Hazard Mater. 185, 401–407.

Oladoja, N.A., Akinlabi, A.K., 2009. Congo red biosorption on palm kernel seed coat. Ind. Eng. Chem. Res. 48, 6188–6196.

Omri, A., Benzina, M., 2012. Removal of manganese (II) ions from aqueous solutions by adsorption on activated carbon derived a new precursor: Ziziphus spina-christi seeds. Alexandria Eng. J. 51, 343–350.

Prelot, B., Araïssi, M., Gras, P., Marchandeau, F., Zajac, J., 2018. Contribution of calorimetry to the understanding of competitive adsorption of calcium, strontium, barium, and cadmium onto 4A type zeolite from two-metal aqueous solutions. Thermochim. Acta 664, 39.

Ravikovitch, P.I., Neimark, A.V., 2002. Experimental confirmation of different mechanisms of evaporation from ink-bottle type pores:Equilibrium ,pore blocking ,and cavitation. Langmuir 18 (25), 9830–9837.

Ren, X., Chen, C., Nagatsu, M., Wang, X., 2011. Carbon nanotubes as adsorbents in environmental pollution management: a review. Chem. Eng. J. 170, 395–410.

Samadi, N., Hasanzadeh, R., Rasad, M., 2015. Adsorption isotherms, kinetic, and desorption studies on removal of toxic metal ions from aqueous solutions by polymeric adsorbent. J. Appl. Polym. Sci. 132.

Sanad, S.A., Moniem, S.M., Abdel-Latif, M.L., Hossein, H.A., El-Mahllawy, M.S., 2021. Sustainable management of basalt in clay brick industry after its application in heavy metals removal. J. Mater. Res. Technol. 10, 1493–1502.

Sayed, M., Abbas, M., Abdel Moniem, S.M., Ali, M.E.M., Naga, S.M., 2019. Facile and room temperature synthesis of superparamagnetic Fe_3O_4/C core/shell nanoparticles for efficient removal of Pb (II) from aqueous solution. Chemistry Select 4 (6), 1857–1865. .

Selles-Perez, M.J., Martin-Martinez, J.M., 1991. Application of α and n plots to N_2 adsorption isotherms of activated carbon. Chem. Soc. Farad. Trans. 87, 1237–1243.
Sharaky, A.M., El Hasanein, A.S., Atta, S.A., Khallaf, K.M., 2016. Part II groundwater in the nile Delta nile and groundwater interaction in the western nile Delta, Egypt. In: The Handbook of Environmental Chemistry Founded by Otto Hutzinger Editors-in-Chief: Damià Barceló, Andrey G. Kostianoy Volume 55, pp. 33–62.
Shi, T., Jia, S., Chen, Y., Wen, Y., Du, C., Guo, H., Wang, Z., 2009. Adsorption of Pb(II), Cr(III), Cu(II), Cd(II) and Ni(II) onto a vanadium mine tailing from aqueous solution. J. Hazard Mater. 169 (1–3), 838–846.
Shouman, M.A., Fathy, N.A., 2018. Microporous nanohybrids of carbon xerogels and multi-walled carbon nanotubes for removal of rhodamine B dye. J. Water Proc. Eng. 23, 165–173.
Sun, K., Jiang, J.C., Jun-ming, X., 2009. Chemical regeneration of exhausted granular activated carbon used in citric acid fermentation solution decoloration. Iran J. Chem. Chem. Eng. (IJCCE) 28 (4), 79–83.
Temkin, M.J., Pyzhev, V., 1940. Recent modifications to langmuirisotherms. Acta Physicochim. USSR 12, 217–222.
Tolkou, A.K., Katsoyiannis, I.A., Zouboulis, A.I., 2020. Removal of arsenic, chromium and uranium from water sources by novel nanostructured materials including graphene-based modified adsorbents: a mini review of recent developments. Appl. Sci. 10, 1–18, 3241.
Verhave, B., Goldberg, M., Hashim, P., Levitt, J., 2019. Treatment of arsenic-induced Bowen's disease with topical 5-fluorouracil. J. Drugs Dermatol. 18 (5), 477–479.
Visa, M., 2016. Synthesis and characterization of new zeolite materials obtained from fly ash for heavy metals removal in advanced wastewater treatment. Powder Technol. 294, 338–347.
Wang, H., Liu, Y.G., Zeng, G.M., Hu, X.J., Hu, X., Li, T.T., Li, H.Y., Wang, Y.Q., Jiang, L.H., 2014. Grafting of beta-cyclodextrin to magnetic graphene oxide via ethylenediamine and application for Cr(VI) removal. Carbohydr. Polym. 113, 166–173.
Wang, C., Yang, S., Ma, Q., Jia, X., Ma, P.-C., 2017. Preparation of carbon nanotubes/graphene hybrid aerogel and its application for the adsorption of organic compounds. Carbon 118, 765–771.
Wang, Y., Pan, C., Chu, W., Vipin, A.K., Sun, L., 2019. Environmental remediation applications of carbon nanotubes and graphene oxide: adsorption and catalysis. Nanomaterials 9, 1–25.
WHO, 2008. Guidelines for Drinking Water Quality. World Health Organization, Geneva.
Xu, D., Tan, X.L., Chen, C.L., Wang, X.K., 2008. Adsorption of Pb(II) from aqueous solution to MX-80 bentonite: effect of pH, ionic strength, foreign ions and temperature. Appl. Clay Sci. 41 (1-2), 37–46.
Xu, R., Chen, M., Fang, T., Chen, J., 2017. A new method for extraction and heavy metals removal of abalone visceral polysaccharide. J. Food Process. Preserv. 41, e13023.
Xu, J., Cao, Z., Zhang, Y., Yuan, Z., Lou, Z., Xu, X., Wang, X., 2018. A review of functionalized carbon nanotubes and graphene for heavy metal adsorption from water: preparation, application, and mechanism. Chemosphere 195, 351–364.
Yang, X., Wan, Y., Zheng, Y., He, F., Yu, Z., Huang, J., Wang, H., Ok, Y.S., Jiang, Y., Gao, B., 2019. Surface functional groups of carbon-based adsorbents and their roles in the removal of heavy metals from aqueous solutions: a critical review. Chem. Eng. J. 366, 608–621.
Zhao, C., Ge, R., Zhen, Y., Wang, Y., Li, Z., Shi, Y., Chen, X., 2019. A hybrid process of coprecipitation-induced crystallization-capacitive deionization-ion exchange process for heavy metals removal from hypersaline ternary precursor wastewater. Chem. Eng. J. 378, 122136.